

Turbulence and Transport Suppression Scaling with Flow Shear on the Large Plasma Device

D.A. Schaffner,¹ T.A. Carter,¹ G.D. Rossi,¹ D.S. Guice,¹ J.E. Maggs,¹ S. Vincena,¹ and B. Friedman¹

*Department of Physics and Astronomy, University of California,
Los Angeles*

(Dated: 14 December 2012)

Continuous control over azimuthal flow and shear in the edge of the Large Plasma Device (LAPD) [W. Gekelman, *et. al*, Rev. Sci. Instr. **62**, 2875 (1991)] has been achieved using a biasable limiter. This flow control has allowed a careful study of the effect of flow shear on pressure-gradient-driven turbulence and particle transport in LAPD. The combination of externally-controllable shear in a turbulent plasma along with the detailed spatial diagnostic capabilities on LAPD makes the experiment a useful testbed for validation of shear suppression models. Motivated by these models, power-law fits are made to the density and radial velocity fluctuation amplitudes, particle flux, density-potential crossphase and radial correlation length. The data show a break in the scaling these quantities with shearing at around a normalized shearing rate of one (shearing rate (γ_s) equal to the turbulent decorrelation rate ($1/\tau_{ac}$)). No one model captures the trends in the data across all values of shearing, but some models successfully match the trend in either the weak ($\gamma_s \tau_{ac} < 1$) or strong shearing limits ($\gamma_s \tau_{ac} > 1$).

I. INTRODUCTION

Suppression of turbulence and turbulent transport by flow shear has been observed on a multitude of different magnetized plasma experiments^{1–6}. While the importance of cross-field flow shear for the successful high confinement operation of fusion devices is well recognized⁷, we still lack a fully first-principles understanding of how sheared flow regulates turbulence and transport. The development of this understanding is essential in the development of a predictive capability for transport for current and future devices such as ITER. Experimental validation of shear suppression models is a critical part of this development process, providing motivation for experiments in which the response of turbulence to shear flow is carefully documented. External control of flow shear in a magnetized plasma has been previously achieved in a number of toroidal devices using biased electrodes to drive cross-field currents and torque to drive plasma rotation^{8,9}. Transport reduction and confinement transitions have been observed and this response has been compared to models for shear suppression, in particular from TEXTOR^{10–12}.

Biasing has been used to induce rotation and transitions in particle confinement in the Large Plasma Device (LAPD)[?] [?]. A recent dataset on LAPD⁶, where a detailed scan of sheared flow in a turbulent, linear field line plasma was made using a biased limiter, is used to extend such shear suppression model verification studies. The recent data set demonstrated the suppression and modification of a number of turbulent quantities with increased shearing rate including cross-field particle flux, density and radial $E \times B$ velocity fluctuations, the relative crossphase between said fluctuations, and radial correlation length. Moreover, the scan included data points in both the weak and strong shearing regime, as defined by the ratio of shearing rate to inverse autocorrelation time providing the ability for comparison to models which make separate predictions for each regime.

Models based on radial decorrelation of turbulent structures by shear are prominent and have been the most theoretical common approach to describing both the physical mechanism underlying suppression as well as for making scaling predictions³. The basic premise underlying these models is the tendency of shearing to break apart or shrink turbulent eddies and consequently decrease both fluctuation amplitude and transport step size. Variation in the model predictions arise from differences in shearing level (strong vs weak), source of turbulent drive (i.e. Ion Temperature Gradient, Interchange Drive or Pressure-Gradient Drive),

as well as consideration of passive versus dynamic scalars. Recently, other approaches to explaining shear suppression have been made including the enhancement of coupling to damped eigenmodes through zonal flows¹⁴ and by nonlinear shifts in the wavenumber spectrum of the turbulence by shearing¹⁵. However, this paper will focus on the varying decorrelation models which include scaling predictions.

This paper presents experimental fits of density fluctuation amplitude, radial velocity fluctuation amplitude, particle flux, crossphase, diffusivity and radial correlation length as functions of flow shear and compares them to a number of model predictions for this shear suppression. No one model predicts how all the quantities scale though some models do make favorable comparisons for some quantities, but unfavorable comparisons to others. The fits generally show a stronger decrease in turbulent fluctuations than crossphase as a contributor to reduction of particle flux. Fits to the suppression of measured radial diffusion—which incorporates the changes in density gradient—compare well to numerical simulation predictions. The ability to make favorable predictions for some quantities while not other perhaps suggests a dependence on turbulent conditions for determining shear suppression and call for specific calculations for LAPD plasmas to be made.

The remainder of this paper will first look at the various models of shear suppression in Section II, then move on to a brief review of the limiter biased rotation studies on LAPD in Section III. In Section IV, the approach for model fitting of the experimental data is discussed and the results of these fits are presented in Section V. Finally a discussion of how these fits compare to analytic and simulation model predictions is given in Section VI.

II. MODELS OF SHEAR SUPPRESSION

Two of the earliest models of shear suppression were decorrelation models developed by Biglari, Diamond, Terry¹⁶ (hereafter BDT) and Shaing¹⁷. The BDT theory presents a generalized analysis of the transport of a passive scalar in a mean sheared flow in the strong-shear regime with constant turbulent drive (pressure gradient). The BDT model predicts that normalized fluctuation amplitude scales directly with shear to the -2/3 power:

$$\frac{\langle |\tilde{\xi}|^2 \rangle}{\langle |\tilde{\xi}|^2 \rangle_{\gamma_s=0}} \sim (\gamma_s \tau_{ac})^{-2/3} \quad (1)$$

where η can be any quantity such as density or temperature. Conversely, the Shaing model focuses on the weak shearing limit and predicts a scaling of the form:

$$\frac{\langle |\tilde{\xi}|^2 \rangle}{\langle |\tilde{\xi}|^2 \rangle_{\gamma_s=0}} \sim 1 - \alpha(\gamma_s \tau_{ac})^2 \quad (2)$$

Where α is a constant containing mode number information. An attempt to consolidate the BDT and Shaing models was made by Zhang and Mahajan^{18,19} by expanding the model to incorporate the self-consistent modification of the diffusion coefficient and fluctuation spectrum by the flow shear (allowing for a distinction between weak and strong turbulence regimes in the shearing model). The resulting model shows correspondence to the Shaing model in the weak shearing regime while the BDT model is recovered in the strong shearing regime but only for the case where diffusion is unchanged by fluctuation amplitude changes. Furthermore, they extend the model to incorporate the effect of changes in gradient scale-length, showing that shear suppression of fluctuation amplitude is enhanced by a steeper equilibrium gradient.

Work by Ware and Terry^{20,21} made predictions for the effect of shearing on particle transport specifically in resistive pressure-gradient driven turbulence. Their work predicted a decrease in flux as $\Gamma_p \sim 1 - \gamma_s^2$ in the weak shear limit. Additionally, the model predicted a decrease in the cosine of the crossphase between density and radial velocity fluctuations of the form $1 - \omega_s^2$. They too incorporated the modification of the pressure gradient, formulating an expression for shearing suppression of radial particle diffusivity of the form:

$$\frac{D}{D(\gamma_s = 0)} \sim 1 - \beta(\gamma_s)^2 \quad (3)$$

where β is a constant containing the linear growth rate and radial mode width.

Further work by Terry, Newman and Ware²² examined the modification of flux in the strong shearing regime for a non-mode-specific turbulence system, predicting a direct scaling of $\Gamma_p \sim \gamma_s^{-4}$ overall, with fluctuation amplitude reduction contributing one power while crossphase reduction contributed three powers of γ_s , suggesting both a strong dependence of flux on shear as well as an implication that the crossphase can be the dominant flux suppression mechanism rather than the fluctuation amplitude. However, Kim and Diamond²³ recast the decorrelation model to include resonance absorption between the shear flow and fluctuations leading to a much weaker dependence of flux on shear, $\Gamma_p \sim \gamma_s^{-1}$, and even weaker dependence of crossphase, $\cos(\theta_{nv}) \sim \gamma_s^{-1/6}$, while fluctuations decreased as $|\tilde{n}|^2 \sim \gamma_s^{-5/3}$.

Additional work²⁴ added the effect of treating the fluctuating flows dynamically in an interchange driven turbulent plasma which allowed for a prediction for the decrease in fluctuating radial velocity as a function of shear scaling as $|\tilde{v}_r|^2 \sim \gamma_s^{-3}$ in weak shear, and $|\tilde{v}_r|^2 \sim \gamma_s^{-4}$ in strong shearing.

Most recently, Leconte et al.²⁵ found different scalings for flux, fluctuations and crossphase in the strong shear regime depending on relative shearing strength relative to a characteristic time and shearing spatial gradient relative to the inhomogeneity gradient. Work by Newton and Kim has utilized numerical simulations to determine shearing scalings in a generic model^{26,27}.

III. SHEAR SUPPRESSION EXPERIMENTS

The Large Plasma Device²⁸ (LAPD) is a 17m long, ~ 60 cm diameter cylindrical plasma produced by a barium-oxide coated nickel cathode. In the experiments reported here, a plasma of density $\sim 2 \times 10^{12} \text{ cm}^{-3}$ and peak temperature of 8eV is produced in a uniform solenoidal magnetic field of 1000G. All measurements reported here were collected using Langmuir probes recording floating potential, V_f , or ion saturation current, I_{sat} . Azimuthal electric field fluctuations, \tilde{E}_θ , are found by taking the simultaneous difference in two V_f signals separated a small azimuthal distance apart. Turbulent particle flux $\Gamma \propto \langle \tilde{n}_e \tilde{E}_\theta \rangle$ is determined through correlating density fluctuations with \tilde{E}_θ where it is assumed that E_θ produces radial $E \times B$ flow. The relative crossphase between fluctuation time-series is determined through the cross-spectrum of the quantities. That is,

$$\theta = \tan^{-1} \frac{\langle Q(f, r) \rangle_{f,r}}{\langle C(f, r) \rangle_{f,r}} \quad (4)$$

where Q and C are the imaginary and real parts of the cross-spectrum, calculated from product of the complex FFTs of the two time-series in question as in,

$$G(f, r) = \hat{x}^*(f, r) \hat{y}(f, r) \quad (5)$$

where the cross-spectrum is first averaged over frequencies to power-weight the crossphase signal, and then averaged radially, before the phase is determined. Finally, steady-state azimuthal flow, V_θ is determined through the radial derivative of plasma potential profiles measured using a swept-Langmuir probe technique again assuming only $E \times B$ flow. The shearing rate is computed as $\gamma_s = d/dr(V_\theta)$.

A large annular aluminum limiter was installed in LAPD to provide a parallel boundary condition for the edge plasma and is biased relative to the cathode of the plasma source to control plasma potential and cross-field flow. A diagram of the limiter arrangement and biasing circuit is shown in Fig. 1.

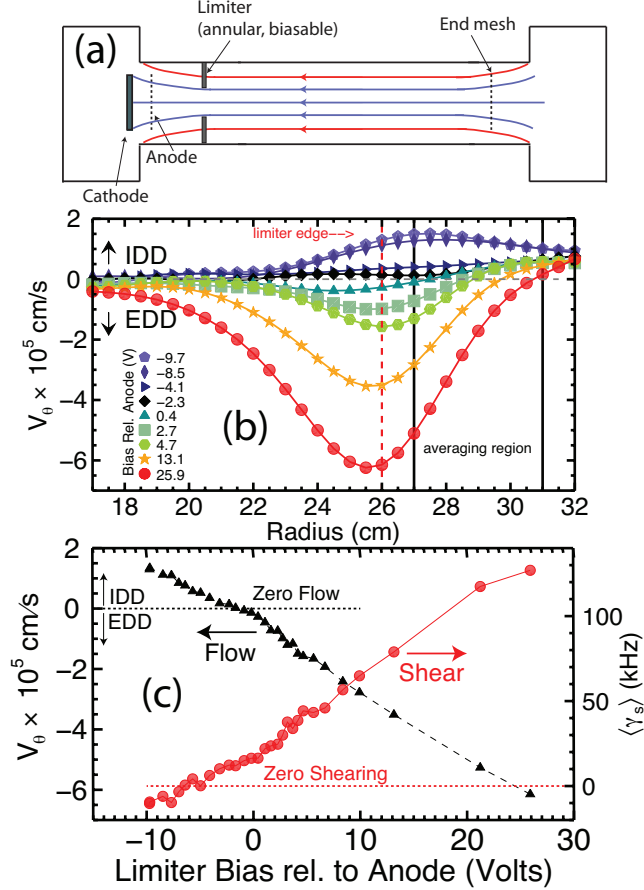


FIG. 1. (a) Diagram of the LAPD device showing annular limiter. (b) Velocity profiles using plasma potential from swept measurements. (c) Flow at the limiter edge (black, triangles) and mean shearing rate, averaged over $27 < r < 31$ cm (red, circles).

A recent experiment on the LAPD demonstrated the ability to achieve continuous control of steady-state azimuthal flow and flow shear through the use of these biasable limiters⁶. Spontaneous rotation is observed in LAPD in the ion diamagnetic direction. This spontaneous flow can be reduced and reversed into the electron diamagnetic direction as the limiter bias is increased. This results in a continuous variation of edge flow and flow shear including zero flow and flow shear states. Shearing rates are achieved up to about five times the turbulent inverse autocorrelation time τ_{ac}^{-1} as measured in the unsheared state. Radial

particle flux and fluctuation amplitude are reduced as shearing rate is increased and the resulting transport changes cause observable steepening of the density gradient. Figure 2 shows the experimental results for measurements of density fluctuation amplitude, radial velocity amplitude and density-radial velocity crossphase as functions of normalized shearing rates. The shearing rates achieved span two regimes: a weak-shear regime where $\gamma_s \tau_{ac} < 1$ and a strong-shear regime where $\gamma_s \tau_{ac} > 1$. The blue solid lines correspond to the best fits for the strong-shear cases while the green are the best fits for the weak-shear case. Similar plots for particle flux and diffusivity $D = \Gamma/|\nabla n|$ are shown in Fig. 3. Error bars of $\pm 20\%$ for each quantity are shown on the plots and used in the fits, reflecting a statistical error from the number of shots used to average the quantity ($\sigma \sim 1/\sqrt{nshots}$).

Measurements of the radial correlation length were recorded as a function of shearing rate (applied bias) using a two-probe correlation technique. A reference probe collecting I_{cmrsat} is kept stationary at a particular axial and radial location within LAPD. A second Langmuir probe situated at an axial point closer to the cathode is moved shot-to-shot in a rectangular grid around the radial location of the reference probe. The cross-field cross-correlation function of these two measurements is computed shot-to-shot for a delay time τ as $C(x, y, \tau) = \langle I_{ref}(x, y, t) I_{mot}(x, y, t + \tau) \rangle$. Fig. 4(a) shows the normalized correlation function $C(x, y)/C_{max}$ for the unbiased state (flow in the IDD), a minimum shear state, and a high bias state (large EDD flow) with a reference probe located at $x = 29.5\text{cm}$, $y = 0\text{cm}$ (right in the middle of the shear layer). The black curve represents the contour line where $C(x, y)/C_{max} = 0.5$. The radial correlation length Δr_c is defined here as the radial width of this black curve through the reference probe location. The variation of the correlation length versus shearing rate is shown in Fig. 4 (normalized to the maximum radial correlation length calculated for all biases). The correlation length is found to decrease substantially with shearing. A break in the trend of decreasing correlation length is observed for larger shearing rates where the correlation function appears to be dominated by a coherent mode (which also appears in the temporal power spectrum).

Some achieved parameters regimes for the shearing rate and density gradient length scales are presented in Fig. 5. The shearing scale length is calculated as in $L_\gamma = |\nabla \ln(v_{E \times B})|^{-1}$. This value is compared to the density gradient scale length, $L_n = |\nabla \ln n|^{-1}$ for each bias and mapped to a normalized shearing value. This plot shows that for all of the strong shearing regime, and nearly half of the weak shearing regime, $L_n > L_\gamma$. The reverse is true

only for the weakest shearing points. This quantity L_γ/L_n can be utilized in asymptotic limits similar to the γ_s/τ_{ac}^{-1} ratio for models²⁵.

IV. EXPERIMENTAL SHEAR SUPPRESSION SCALING

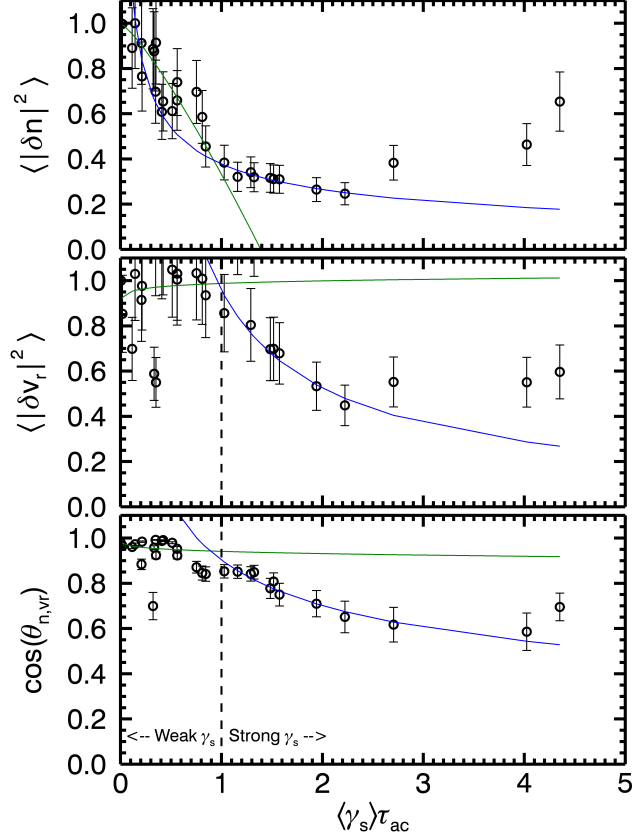


FIG. 2. Scaling of (a) density fluctuation amplitude, (b) radial velocity fluctuation amplitude, and (c) relative crossphase between density and radial velocity fluctuations. Density and velocity fluctuation are each normalized to the value at minimum shear. The green curves correspond to $1 - \gamma_s^\nu$ fits of the weak shear regime with $\nu = 0.501$ for flux and $\nu = 0.418$ for D. The blue curves correspond to γ_s^ν fits with $\nu = -1.719$ for flux and $\nu = -1.646$ for D.

The variation of the experimentally measured quantities with normalized shearing rate was fit to functions motivated by models discussed above: functions of the form $1 - \gamma_s^\nu$ (hereafter M1 or model type 1) and of γ_s^ν (hereafter M2). For model type 1, the measured quantity, y , was normalized to the value at zero shear, then transformed as $-(1 - y)$. Then, taking the logarithm of both sides, a linear fit was made for points in the weak shear and

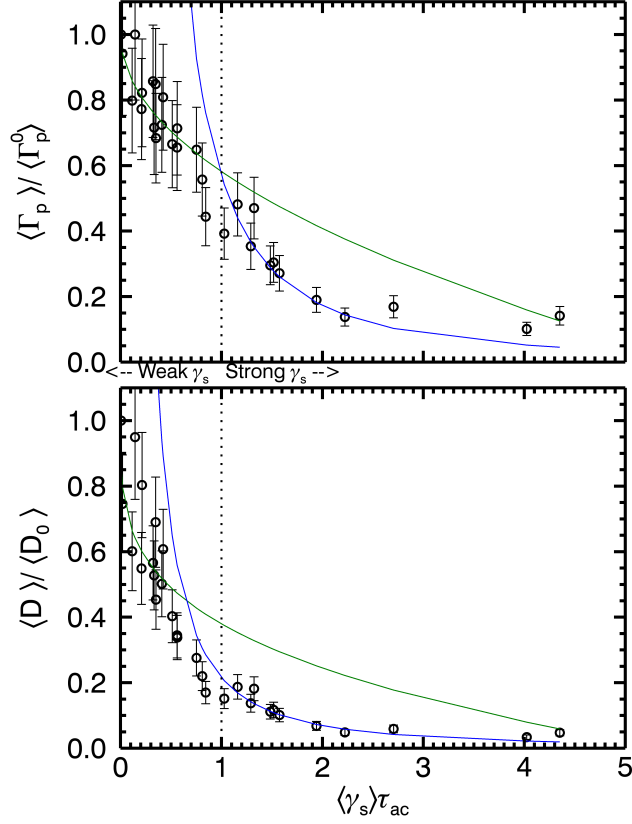


FIG. 3. Scaling of (a) radial particle flux and (b) diffusion coefficient each normalized to the value at minimum shear, $\Gamma_p^0 = 1.7 \times 10^{16} \text{cm}^{-2}$ and $D_0 = 36.7 \text{m}^2/\text{s}$. The green curves correspond to $1 - \gamma_s^\nu$ fits of the weak shear regime with $\nu = 0.501$ for flux and $\nu = 0.418$ for D. The blue curves correspond to γ_s^ν fits with $\nu = -1.719$ for flux and $\nu = -1.646$ for D.

TABLE I. Power-law fits for $|\tilde{n}^2|$ scaling with shear for frequencies in 350Hz to 100kHz. Model form refers to how the shearing relates to the quantity in question, with C a constant and ν the power exponent.

Model form	γ_s regime	ν	χ^2	χ^2/ndf
$\sim 1 - C\gamma_s^\nu$	$\gamma_s \tau_{ac} < 1$	1.228	1.091	0.0642
$\sim 1 - C\gamma_s^\nu$	$\gamma_s \tau_{ac} > 1$	0.231	0.0332	0.0037
$\sim C\gamma_s^\nu$	$\gamma_s \tau_{ac} < 1$	-0.116	0.1791	0.0094
$\sim C\gamma_s^\nu$	$\gamma_s \tau_{ac} > 1$	-0.512	0.0024	0.0003

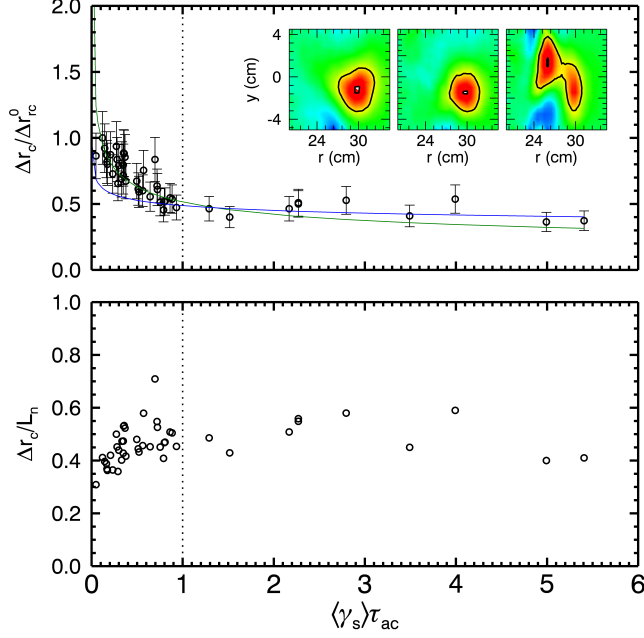


FIG. 4. (a)Radial correlation length normalized to maximum correlation length versus normalized shearing rate with correlation planes of unbiased, zero shear, and high bias states in the inset. (b)Ratio of radial correlation length to density gradient scale length.

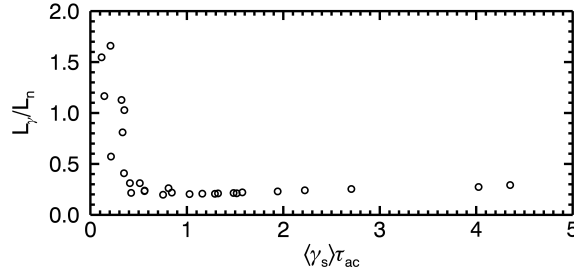


FIG. 5. Ratio of shearing length scale to density gradient length scale versus normalized shearing in the radial region of 27 to 31cm.

TABLE II. Power-law fits for $|\hat{v}_r^2|$ scaling with shear for frequencies in 350Hz to 100kHz. Model form refers to how the shearing relates to the quantity in question, with C a constant and ν the power exponent.

Model form	γ_s regime	ν	χ^2	χ^2/ndf
$\sim C\gamma_s^\nu$	$\gamma_s\tau_{ac} < 1$	0.016	0.2121	0.0117
$\sim C\gamma_s^\nu$	$\gamma_s\tau_{ac} > 1$	-0.866	0.0037	0.0005

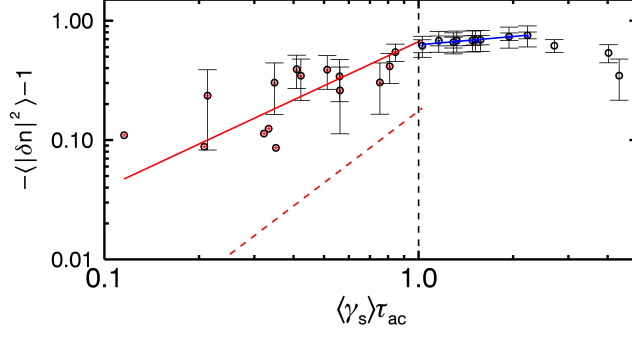


FIG. 6. Log-Log plot of $-(\text{density fluctuation amplitude})^{-1}$ versus shearing with fit function for weak shear in solid red, Shaing scaling of 2 indicated by dashed red line. Blue line is fit for strong shearing

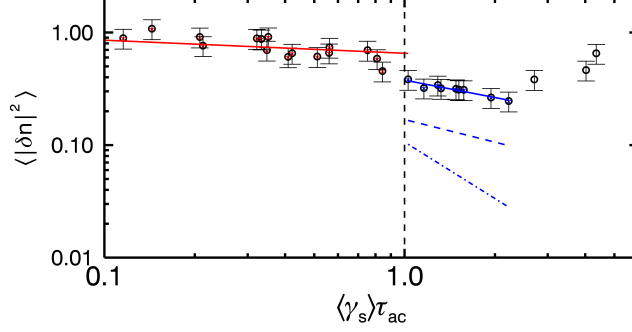


FIG. 7. Log-Log plot of density fluctuation amplitude versus shearing with fit function for strong shear in solid blue, BDT scaling of $-2/3$ indicated by dashed blue line and Kim and Diamond scaling of $-5/3$ indicated by steeper dashed-dotted line.

TABLE III. Power-law fits for Γ_p scaling with shear for frequencies in 350Hz to 100kHz. Model form refers to how the shearing relates to the quantity in question, with C a constant and ν the power exponent.

Model form	γ_s regime	ν	χ^2	χ^2/ndf
$\sim 1 - C\gamma_s^\nu$	$\gamma_s \tau_{ac} < 1$	0.501	0.332	0.0189
$\sim 1 - C\gamma_s^\nu$	$\gamma_s \tau_{ac} > 1$	0.638	0.923	0.103
$\sim C\gamma_s^\nu$	$\gamma_s \tau_{ac} < 1$	-0.111	0.146	0.0077
$\sim C\gamma_s^\nu$	$\gamma_s \tau_{ac} > 1$	-1.719	6.54	0.726

TABLE IV. Power-law fits for $\cos(\theta_{nv_r})$ scaling with shear for frequencies in 350Hz to 100kHz. Model form refers to how the shearing relates to the quantity in question, with C a constant and ν the power exponent.

Model form	γ_s regime	ν	χ^2	χ^2/ndf
$\sim 1 - C\gamma_s^\nu$	$\gamma_s\tau_{ac} < 1$	0.226	6.1140	0.3320
$\sim C\gamma_s^\nu$	$\gamma_s\tau_{ac} < 1$	-0.020	0.0369	0.0019
$\sim C\gamma_s^\nu$	$\gamma_s\tau_{ac} > 1$	-0.365	0.0023	0.0003

in the strong shear separately. The resulting slope of the fit is taken as the power ν . For M2, no transformation of the quantity y to $-(1 - y)$ is made before taking the logarithm and fitting. For a complete comparison to the wide range of model predictions made, fits were made for density fluctuation amplitude, radial particle flux, density-radial velocity fluctuation crossphase, radial velocity (ExB) fluctuation amplitude, radial correlation length, and experimentally determined diffusivity ($\Gamma/|\nabla n|$). The best fits are summarized in Table I-VI for each model type and for both weak and strong shearing. The χ^2 and χ^2/ndf (where ndf is the number of degrees of freedom) is also indicated in the tables. For weak shear fits, all points less than the weak shear cutoff $\gamma_s\tau_{ac}|1$ are used in the fit. For strong shear, all but the last three points are used. The last points appear to be strongly influenced by the presence of a coherent mode that develops in the highest shear and flow cases and is thought to be a break from the scaling observed in the strong shear regime. For quantities determined by averaging over frequency (e.g. density and velocity fluctuation amplitudes, flux and diffusivity) the frequency band used was 350Hz to 100kHz.

The log-log plots highlight the break in trend between weak and strong shear. It should also be noted that in this dataset, the density steepening that occurs due to the decreased transport as reported in⁷ saturates just before the transition between weak and shear regimes and may also play a role in the differing trends.

TABLE V. Power-law fits for $D = \Gamma_p/\nabla n$ scaling with shear for frequencies in 350Hz to 100kHz. Model form refers to how the shearing relates to the quantity in question, with C a constant and ν the power exponent.

Model form	γ_s regime	ν	χ^2	χ^2/ndf
$\sim 1 - C\gamma_s^\nu$	$\gamma_s\tau_{ac} < 1$	0.418	1.4710	0.0817
$\sim 1 - C\gamma_s^\nu$	$\gamma_s\tau_{ac} > 1$	0.197	0.0016	0.0002
$\sim C\gamma_s^\nu$	$\gamma_s\tau_{ac} < 1$	-0.217	0.4200	0.0221
$\sim C\gamma_s^\nu$	$\gamma_s\tau_{ac} > 1$	-1.646	0.0187	0.0021

TABLE VI. Power-law fits for Δr_c scaling with shear for frequencies in 350Hz to 100kHz. Model form refers to how the shearing relates to the quantity in question, with C a constant and ν the power exponent.

Model form	γ_s regime	ν	χ^2	χ^2/ndf
$\sim C\gamma_s^\nu$	$\gamma_s\tau_{ac} < 1$	-0.290	5.8730	0.1630
$\sim C\gamma_s^\nu$	$\gamma_s\tau_{ac} > 1$	-0.113	3.7040	0.3370

V. RESULTS

A. Density and Velocity Fluctuations

The best fits for scaling of density fluctuation amplitude are shown in Table I. For the weak shear regime, the χ^2 values suggest M2 to be a slightly better model fitting model than M1. Though M1 is not used for prediction of strong shear scaling in the literature, a fit was made to it here for completeness; still, as with the weak shearing regime, values of χ^2 show M2 to be a better model for the strong shearing regime as well.

The $\nu = -0.512$ fit for strong shearing M2 is reasonably close to the BDT prediction of $-(2/3)$. However, it should be reiterated that BDT assumes a fixed turbulence drive and that in this dataset, the gradient scale length decreases substantially as shearing is increased, resulting in an increase in turbulent drive. This actually implies a stronger than BDT scaling of fluctuation amplitude suppression overall, despite the smaller exponent. For weak shearing M2, the experimental fit of $\nu = -0.116$ also suggests weaker scaling than the M2 prediction by Kim and Diamond of $-(2/3)$.

A prediction for the scaling of radial velocity fluctuation amplitude is only made by Kim and Diamond²⁴ in the dynamically evolved case. Fits, listed in Table II, suggest a much weaker scaling than predicted for both weak and strong shear. The weak shear fit actually shows a slight increase in fluctuation amplitude rather than a $\nu = -3$ scaling while in the strong shear regime a fit of $\nu = -0.866 \ll -4$ is found.

B. Flux and Diffusivity

Particle flux and diffusivity fits and χ^2 results are shown in Table III and V respectively. Like density fluctuations, M2 is the slightly better model than M1 for weak shear based on χ^2 values; however, for strong shear, the M1 model actually has a much better fit than the M2 model, though M1 is not derived in the strong shearing limit in the literature. Despite the higher χ^2 , the fit of $\nu = -1.719$ falls in between the extremes of predictions of $\nu = -1$ and $\nu = -4$. The weak shear fit of $\nu = -0.111$ falls far short of the Kim and Diamond M2 prediction of $\nu = -2$. In addition to being the less well-fitted model, the predicted exponent for the M1 weak shearing is also far less than the Terry and Ware value of $\nu = 2$.

Diffusivity, like flux, has the lower χ^2 values for M2 with weak shearing and for M1 with strong shearing. The only predictions for D come from Terry and Ware using M1 as shown earlier in this paper and a numerical simulation result from Newton and Kim²⁷ for evolved turbulence with a finite correlation time. The experimental fit of $\nu = 0.418$ again falls short of the predicted $\nu = 2$, though the strong M2 fit of $\nu = -1.646$ is fairly close to the calculated value of $\nu = -1.75$.

C. Crossphase and Correlation Length

Fits for the scaling of cosine of the crossphase between density and radial velocity fluctuations is shown in Table IV. M2 is the better fitting model than M1 for both weak and strong shearing. The weak M2 fit of $\nu = -0.02$ and strong M2 fit of $\nu = -0.365$ both tend to support the prediction of mild scaling with crossphase made by Kim and Diamond^{23,24} with $\nu = -(1/6)$ rather than the large scaling of $\nu = -3$ made by Terry²².

Finally, a fit to radial correlation length is made and compared to the only explicit prediction made by BDT¹⁶. Neither the weak shear fit of $\nu = -0.290$ nor the strong shear of

$\nu = -0.113$ is unreasonably far from the predicted value of $\nu = -1/3$ though the χ^2 values do not suggest a great fit to the model. It should again be noted that these correlation lengths are measured in the steady-state period when the density gradient scale length will have already adjusted due to the change in transport. Thus, this decrease in radial correlation length could be more directly due to steady-state gradient scale length rather than shearing. In Figure 4(b) the ratio of the radial correlation length to the density gradient scale length is shown to remain constant with shearing. This suggests that the correlation length could be adjusting to the gradient scale length and that a scaling with shearing rate could be indirect. In order to truly evaluate the effect of shearing on radial correlation length, the quantity should be measured before changes to the density gradient occur. This can conceivably be done by examining plasma quantities in time rather averaging in the steady-state and will be looked at in a future paper.

VI. DISCUSSION

While the large variation in fits of shear suppression for six turbulent quantities makes careful model validation difficult, there are a number of conclusions that can be drawn from this analysis. First both analytic predictions and the experimental results from this dataset show a distinct difference in scaling between the weak and strong shear regimes. Second, the models that predict scaling as γ_s^ν in general better fit the data based on χ^2 values than models of the form $1 - \gamma_s^\nu$ with an exception noted in the case of flux and diffusivity. Third, the data clearly supports the prediction that density fluctuation amplitude is more strongly suppressed than cosine of the crossphase and thus makes a more significant contribution to the suppression of radial transport. Fourth, the fairly weak velocity fluctuation scaling with shear suggests that the dynamic modeling of the flow may not be that important in LAPD plasmas. Finally, as indicated by the wide range of predictions, the scaling of shear suppression may be dependent on the nature of the turbulence at hand. Many of the turbulence models are mode specific such as pressure-gradient turbulence for the Terry, Ware models or Rotational interchange for the later Kim, Diamond models. However, neither model fits the LAPD results very well which itself is likely a combination of pressure-gradient and rotational interchange turbulence. For future model development and comparison to these results, it may be worthwhile to make predictions based on specific LAPD type turbulence.

VII. CONCLUSIONS

The results of this paper present power-law fits of experimental measurements of density fluctuations, radial velocity fluctuations, particle flux, crossphase, diffusivity and radial correlation length as a function of both weak and strong shearing as found on the LAPD. These results are compared to the myriad of models for prediction of shear suppression which are based on the physical idea of shear decorrelation of turbulent eddies. While some of the model predictions approach the experimentally measured values, most are only capable of being close to only one or two of the predicted quantities while generally far off on others. In the process of developing these analytic shear suppression models, assumptions must often be made about the type of turbulence involved (such as pressure-gradient driven turbulence versus rotational interchange driven turbulence) when it is likely, rather, that many types of free-energy are available in the actual experimental plasma (as on the LAPD where both drift waves and rotational interchange modes may be present). Simulation work which can incorporate more complex turbulent environments, then, could in this vein have some promise for better matching to experiment as well as analytical endeavors to develop a shear suppression model specifically for LAPD plasma. Lastly, there is, of course, the possibility that decorrelation models are not the correct models for predicting shear suppression. Comparison of this dataset to predictions made by alternative shear suppression models, such as suppression by shifted radial wavenumbers[?], will be made in future work.

REFERENCES

- ¹K. Burrell, Phys. Plasmas **4**, 1499 (1997).
- ²K. Burrell, Phys. Plasmas **6**, 4418 (1999).
- ³P. Terry, Rev. Mod. Phys. **72**, 109 (2000).
- ⁴G. Van Oost, J. Adamek and V. Antoni, P. Balan, J.A. Boedo, P. Devynck, I. Duran, L. Eliseev, J.P. Gunn, M. Hron, C. Ionita, S. Jachmich, G.S. Kirnev, E. Martines, A. Melnikov, R. Schrittwieser, C. Silva, J. Stockel, M. Tendler, C. Varandas, M. Van Schoor, V. Vershkov and R.R. Weynants, Plas. Phys. Control Fusion **48**, 621 (2003).
- ⁵O. Sakai, Y. Yasaka and R. Itatani, Phys. Rev. Lett. **70**, 4071 (1993).

- ⁶D.A. Schaffner, T.A. Carter, G.D. Rossi, D.S. Guice, J.E. Maggs, S.Vincena and B. Friedman, Phys. Rev. Lett. **109**, 135002 (2012).
- ⁷K.H. Burrell, T.N. Carlstrom, E.J. Doyle, D. Finkenthal, P. Gohil, R.J. Groebner, D.L. Hillis, J. Kim, H. Matsumoto, R.A. Moyer, T.H. Osborne, C.L. Rettig, W.A. Peebles, T.L. Rhodes, H. St.John, R.D. Stambaugh, M.R. Wade and J.G. Watkins, Plas. Phys. Control Fusion **34**, 1859 (1992).
- ⁸R.J. Taylor, M.L. Brown, B.D. Fried, H. Grote, J.R. Liberati, G.J. Morales, P. Pribyl, D. Darrow and M. Ono, Phys. Rev. Lett. **63**, 2365 (1989).
- ⁹R.R. Weynants, G. Van Oost, G. Bertschinger, J. Boedo, P. Brys, T. Delvigne, K.H. Dippel, F. Durodie, H. Euringer, K.H. Finken, D.S. Gray, J.D. Hey, D.L. Hillis, J.T. Hogan, L. Konan, R. Leners, A.M. Messiah, A. Pospieszczyck, U. Samm, R.P. Schorn, B. Schweer, G. Telesca, R. Vannieuwenhove and P.E Vandenplas, Nucl. Fusion **32**, 837 (1992).
- ¹⁰R.R. Weynants, S. Jachmich and G. Van Oost, Plas. Phys. Control Fusion **40**, 635 (1998).
- ¹¹J. Boedo, D. Gray, S. Jachmich, R. Conn, G.P. Terry, G. Tynan, G. Van Oost, R.R. Weynants and TEXTOR Team, Nucl. Fusion **40**, 7 (2000).
- ¹²J.A. Boedo, D.S. Gray, P.W.Terry, S. Jachmich, G.R. Tynan, R.W. Conn and TEXTOR-94 Team, Nucl. Fusion, **42**, 117 (2002).
- ¹³B. Friedman, T.A. Carter, M.V. Umansky, D. Schaffner and B. Dudson, Phys. Plasmas **19**, 102307 (2012).
- ¹⁴P.W. Terry and R. Gatto, Phys. Plasmas **13**, 062309 (2006).
- ¹⁵G.M. Staebler, R.E. Waltz, J.E. Kinsey and W. Solomon in *Proceedings of the 24th Fusion Energy Conference, San Diego, 2012* (International Atomic Energy Agency, Vienna, 2012).
- ¹⁶H. Biglari, P.H. Diamond and P.W. Terry, Phys. Fluids B. **2**, 1 (1990).
- ¹⁷K.C. Shaing, E.C. Crume and W.A. Houlberg, Phys. Fluids B **2**, 6 (1990).
- ¹⁸Y.Z. Zhang and S.M. Mahajan, Phys. Fluids B **4**, 1385 (1992).
- ¹⁹Y.Z. Zhang and S.M. Mahajan, Phys. Fluids B **5**, 7 (1993).
- ²⁰A.S. Ware, P.W. Terry, P.H. Diamond and B.A. Carreras, Plasma Phys. Control Fusion **38**, 1343 (1996).
- ²¹A.S. Ware, P.W. Terry, B.A. Carreras and P.H. Diamond, Phys. Plasmas **5**, 173 (1998).
- ²²P.W. Terry, D.E. Newman and A.S. Ware, Phys. Rev. Lett. **87**, 185001 (2001).
- ²³E.-J. Kim and P.H. Diamond, Phys. Rev. Lett. **90**, 7 (2003).

- ²⁴E.-J. Kim and P.H. Diamond, Phys. Plasmas **11**, 10 (2004).
- ²⁵M. Leconte, P. Beyer, S. Benkadda and X.Garbet, Phys. Plasmas **13** 112301 (2006).
- ²⁶A.P.L. Newton and E.-J. Kim, Phys. Plasmas **14**, 122306 (2007).
- ²⁷A.P.L. Newton and E.-J. Kim, Phys. Plasmas **18**, 052305 (2011).
- ²⁸W. Gekelman, H. Pfister, Z. Lucky, J. Bamber, D. Leneman and J. Maggs, Rev. Sci. Instrum. **62**, 2875 (1991).